

Bound states in the continuum of higher-order topological insulators

Wladimir A. Benalcazar and Alexander Cerjan

Department of Physics, The Pennsylvania State University, University Park, Pennsylvania 16802, USA

(Dated: April 9, 2024)

We show that lattices with higher-order topology can support corner-localized bound states even in the absence of a bulk energy gap. Topological bound states in these phases thus constitute condensed matter realizations of bound states in the continuum (BICs). We propose a method for the direct identification of BICs in condensed matter settings and use it to demonstrate the existence of BICs in a concrete lattice model. Although the onset for these states is given by corner-induced filling anomalies in certain topological crystalline phases, additional symmetries are required to protect the BICs from hybridizing with their degenerate bulk states. We analytically demonstrate the protection mechanism for BICs in this model and numerically show how breaking this mechanism transforms the BICs into resonances. Our work shows that topological bulk-boundary correspondences are immune to the existence of interfering bulk bands, expanding the search space for crystalline topological phases.

Topological insulators exhibit robust quantized electromagnetic phenomena with exotic boundary manifestations. A paradigmatic example is the family of topological insulators which manifest quantized dipole moments in their bulk and charge fractionalization at their boundaries [1–3], epitomized by the inversion-symmetric one-dimensional Su-Schrieffer-Hegger model [4]. This property of boundary charge fractionalization has recently been generalized through the discovery of higher-order topological insulators (HOTIs) whose topology is solely protected by crystalline symmetries and which can host corner fractional charges in 2D and 3D [5–14].

Of particular interest is the subset of HOTIs with additional chiral or particle-hole symmetries because they manifest topological corner-bound states at zero energy [5, 7]. These states are constantly sought after because they are easy to access experimentally and show maximal confinement [15–20]. Moreover, in superconductors, they constitute Majorana bound states [21–26]. Both in insulators and superconductors, these states may present interesting braiding properties [27–29].

The current search for materials which are members of this subset (or the construction of metamaterials which are) currently rules out those without a bulk band gap at zero energy. Yet, in principle, spectral isolation is not necessary for the existence of localized bound states. In fact, bound states that coexist with degenerate extended ones, commonly known as bound states in the continuum (BICs), have been found across a variety of other physical systems, including quantum systems [30–33], water waves [34–39], acoustics [40–45], and photonics [46–64].

Thus, the natural question to consider is, do topological crystalline insulators with fractional corner charges still possess corner-localized states in the absence of a gap? And, if so, what protects these states from hybridizing with bulk states at the same energy? If such protected corner-localized modes do exist, they are condensed matter realizations of BICs, as they would be localized to a zero-dimensional region of the system despite

the existence of the background of continuum states in the bulk of the material.

Previous studies on BICs consider systems which are coupled to scattering channels in the surrounding environment that satisfy radiative boundary conditions, rendering their Hamiltonians non-Hermitian by allowing energy to radiate away. In contrast, condensed matter systems, being closed systems, have presented a difficulty in even defining the appropriate criteria for diagnosing the existence of BICs, which only a few previous studies have attempted to address [19, 65, 66].

In this paper, we draw inspiration from open systems to devise a method which allows the identification of BICs in closed crystalline systems. By adding fictitious non-Hermitian terms to the Hamiltonian of the crystal, and in the correct limits, this method diagnoses the existence of BICs in the original system as the isolated states with only purely real energies in the *complex energy spectrum*. Equipped with this tool, we study a concrete model of a 2D HOTI without a bulk gap at zero energy and conclusively demonstrate the existence of zero-energy corner-localized BICs. We further show that the protection of BICs requires more symmetries than those necessary to protect the HOTI phase and that, in the absence of these additional symmetries (but still preserving those which protect the HOTI phase), the BICs mix with their degenerate bulk states to become higher-order topological resonances. Our work shows that bulk-boundary correspondences in topological band theory are general features immune to the existence of interfering bulk bands. Consequently, our work expands the search space for topological phases beyond those with in-gap states to include those hosting higher-order topological resonances or symmetry-protected BICs.

Model and its topological phases. — The lattice we consider is shown in Fig. 1(a) and consists of 4 sites per unit cell with dimerized nearest-neighbor couplings of amplitude 1 (solid lines) and t (dashed lines). For the basis indicated by the numbers in Fig. 1(a), the Bloch Hamil-

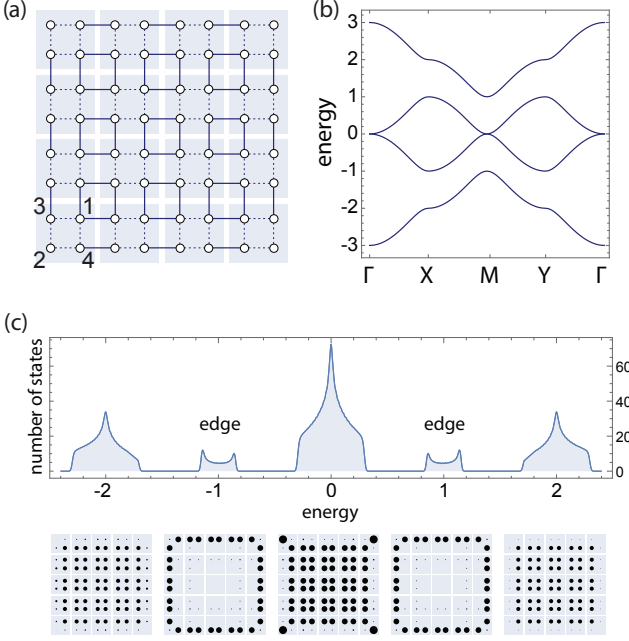


FIG. 1. Model lattice and its topology. (a) Lattice with Hamiltonian in Eq. 1. (b) Bulk energy bands along high-symmetry lines of the Brillouin zone, for $t = 0.5$. (c) Density of states when boundaries are open in both directions ($n = 20$, $t = 0.15$). The lower panels indicate the probability densities per band ($n = 5$, $t = 0.15$).

tonian of the system is

$$h(\mathbf{k}) = \begin{pmatrix} 0 & Q \\ Q^\dagger & 0 \end{pmatrix}, \quad Q = \begin{pmatrix} \gamma + e^{ik_x} & \gamma + e^{ik_y} \\ \gamma + e^{-ik_y} & \gamma + e^{-ik_x} \end{pmatrix}, \quad (1)$$

and its bulk energy bands are shown in Fig. 1(b). This Hamiltonian has chiral symmetry, $\{\Pi, h(\mathbf{k})\} = 0$, where $\Pi = \sigma_z \otimes \mathbb{I}_{2 \times 2}$ is the chiral operator, as well as C_{4v} symmetry. As such, the spectrum is symmetric around zero due to chiral symmetry [see the Supplementary Information (SI)] and the two middle bands are two-fold degenerate at the Γ and \mathbf{M} points of the Brillouin zone as they adopt the 2 dimensional irreducible representation of C_{4v} . Thus, due to the simultaneous presence of chiral and C_{4v} symmetries, the lattice will always have gapless bulk energy bands at zero energy.

The presence of C_{4v} symmetry in the lattice distinguishes two topological phases. For $|t| < 1$, the lattice is in a topological phase, with different C_{4v} (C_{2v}) representations at \mathbf{M} (\mathbf{X} and \mathbf{X}') relative to Γ . On the other hand, for $|t| > 1$, the bands are in a trivial phase, with equal representations at all high symmetry points (HSPs). The symmetry representations at all HSPs for both phases are shown in Table S1 of the SI. At $|t| = 1$, the phase transition occurs by closing both bulk gaps at \mathbf{X} , \mathbf{X}' and \mathbf{M} , exchanging the representations at these three HSPs.

This model has been recently studied in the context of charge fractionalization in higher-order topological crystalline insulators [11]. In the topological phase, the Wannier centers in all the bands localize at the maximal Wyckoff position $1b$ (corner of the unit cell), while in the trivial phase the Wannier centers in all the bands are localized at the maximal Wyckoff position $1a$ (center of the unit cell). The displacement of the Wannier centers relative to the center of their unit cells generates dipole moments per unit length quantized by C_2 symmetry to $\mathbf{P} = (\frac{\epsilon}{2}, \frac{\epsilon}{2})$ in the first and fourth bands of the lattice [11]. These quantized dipole moments are accompanied by two edge energy bands (i.e., bands with edge-localized states) spectrally isolated from the bulk energy bands [Fig. 1(c)].

In addition to the dipole moments, the topological phase has a corner-induced filling anomaly [11] [67], which captures the second-order topological character of the bands. When boundaries are open in both directions, the filling anomaly accounts for a reorganization in the number of states across bands relative to when boundaries are periodic. This reorganization is captured in the probability density functions shown in the lower panel of Fig. 1(c). In particular, the central band shows pronounced support over the corner unit cells and, as we will see, are associated with the existence of corner BICs.

Bound states in the continuum — We can directly test for the existence of corner BICs by dividing the lattice into two regions: a small region that we leave intact which we call the ‘system,’ \mathcal{S} , comprised of the 4 square regions located at the corners, each of size $n_s \times n_s$ unit cells, and a large region called the ‘environment,’ \mathcal{R} , containing all of the unit cells not in \mathcal{S} (inset of Fig. 2). To the environment, we add the non-Hermitian on-site terms

$$h_{loss} = -i\kappa \sum_{\mathbf{r} \in \mathcal{R}} \sum_{\alpha=1}^4 c_{\mathbf{r},\alpha}^\dagger c_{\mathbf{r},\alpha}, \quad 0 < \kappa \ll 1, \quad (2)$$

which amount to uniform losses in all the sites in the environment. If we now inject an initial wave function $\psi(0)$ into the lattice, it will evolve over time as $\psi(t) = e^{-iHt}\psi(0)$ (from now on we set $\hbar = 1$), where H is the Hamiltonian containing both the Hermitian Hamiltonian, Eq. 1, and the non-Hermitian terms, Eq. 2.

Due to the losses in the environment and the fact that all sites in the lattice are coupled, in general we expect $|\psi(t)|^2$ to decrease over time. However, if corner-localized bound states exist in the continuum of the lattice, and for system sizes larger than the exponential confinement of the bound states, the losses of a wave function injected at the bound state will be heavily suppressed. This manifests in the propagator e^{-iHt} by the existence of eigenstates of the Hamiltonian with close-to-real energies and bound to the corners (more precisely, the imaginary component of the complex energy of the bound states should exponentially approach zero with increasing system size).

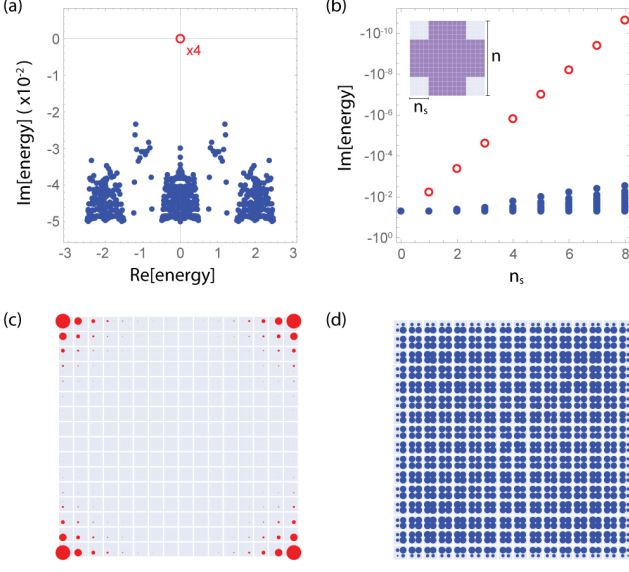


FIG. 2. Probing the existence of bound states in the continuum by adding the non-Hermitian term, Eq. 2, to the lattice in Fig. 1(a) in the topological phase. (a) Complex energies. (b) Imaginary component of the energies as a function of system size (The inset shows the shapes of the ‘system’ and ‘environment’ regions in gray and purple, respectively). In (a) and (b), the red hollow circle is the four-fold degenerate energy of the bound states in the continuum with support at the corners, and the blue solid circles have eigenstates with support in bulk or edges. (c,d) Probability density function of (c) the BICs and (d) the bulk states at zero real energy. In (c) and (d), the area of the circles is proportional to amplitude $|\psi|$ of the states. In (a), (c) and (d), $n = 16$ unit cells, $n_s = 3$ unit cells. In (b) $n = 32$. In all plots, $\kappa = -5 \times 10^{-2}$ and $t = 0.25$.

This exact behavior of the energies of the system is shown in Fig. 2, in which corner-localized bound states are observed in the topological phase of our model. Fig. 2(a) shows the complex energies of the Hamiltonian H , in which four energies are close to being purely real (red hollow circles), while all of the other energies have a non-vanishing imaginary component (blue solid circles). These four nearly-real eigenvalues are shown in Fig. 2(b) to approach a zero imaginary component exponentially fast with increasing system size. As expected, the real energies have eigenstates bound to the corners [Fig. 2(c)]. Crucially, these corner bound states are embedded in the continuum of energies of the central bulk energy band, as can be seen in the cumulative probability density function of all eigenstates with zero real component of the energy other than the four corner bound states, Fig. 2(d).

BICs as a signature of the topological phase — The existence of BICs is exclusive of the topological phase and its associated filling anomaly. When the filling anomaly vanishes, so do the BICs. Figure 3 shows the real and imaginary components of the energies as a function of the hopping amplitude t . In Fig. 3(a), the phase transitions

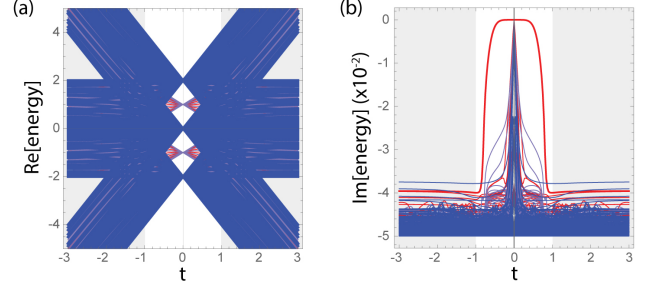


FIG. 3. Complex energies in the lattice as a function of the hopping amplitude t . Shaded and non-shaded regions correspond to the trivial and topological phases, respectively. (a) Real component of the energies. (b) Imaginary component of the energies. Both plots show the overlapped spectra of three configurations: closed boundaries in both directions (blue), closed boundary only along one direction (purple), and open boundaries in both directions (red). Blue spectra is on top of purple spectra, both of which are on top of red spectra. For all plots, $n = 16$, $n_s = 3$, $\kappa = -5 \times 10^{-2}$.

are not visible due to indirect gap closings in the bulk, which start to occur at $t = 0.5$ [Fig. 1(b)].

In the real spectrum [Fig. 3(a)] it is possible to see the appearance of in-gap states in the topological phase when boundaries are open in one direction (green bands). These bands have edge-localized eigenstates. Although the plot shows that the edge states are spectrally separated from the bulk bands only for a fraction of the topological phase, they persist up to the bulk transition point $|t| = 1$.

Here, we focus on corner-bound states because they do not have any spectral isolation at any point of the real energy spectrum and their existence is far from evident. Indeed, we saw that the bound state is embedded in the continuum of the central energy band, and can be separated only in *complex energy* when losses are added to the environment. Under this prescription, only the imaginary component of the spectrum allows the identification of the corner-bound states. These are shown as the red line at zero imaginary energy in the topological phase ($|t| < 1$) in Fig. 3(b). Notice the sharp transition of the BICs into lossy states as the system approaches the phase transition point ($|t| = 1$). In the trivial phase ($|t| > 1$), the BICs are gone as the filling anomaly vanishes.

Symmetry protection of the BICs — The existence of the corner filling anomaly is guaranteed for any spatial symmetry that fixes the Wannier center of the topological phase to the maximal Wyckoff position $1b$, such as C_2 symmetry. However, additional symmetries are required to protect the BICs from mixing with other degenerate bulk states to form resonances. In our model, both C_{4v} and chiral symmetries are required to protect the BICs, as we will show now.

In the bulk, all states at zero energy take the two-

dimensional representation E of C_{4v} (see Table S2 in the SI). Degenerate to these are the four corner states which, as a whole, form the representation $A_1 \oplus B_2 \oplus E$. The A_1 and B_2 corner states cannot mix with the E bulk states as they have incompatible symmetry representations. However, the E corner and E bulk states can in principle mix. Consider the combinations of corner states $|C_+\rangle = \frac{1}{2}(1, -1, i, -i)^T$ and $|C_-\rangle = \frac{1}{2}(1, -1, -i, i)^T$ that form a basis for the E irreducible representation of corner states, where the entries correspond to the corner states localized at the top right, bottom left, top left, and bottom right corners, respectively. Since $|C_\pm\rangle$ are a basis for a 2D irrep, they are degenerate in energy as long as C_{4v} is preserved. This basis is convenient because, in the presence of chiral symmetry, $|C_\pm\rangle$ are chiral partners of each other, i.e., $|C_+\rangle = \Pi|C_-\rangle$ and viceversa, from which it follows that these two states should have energies of opposite sign, $\epsilon, -\epsilon$ (see SI). Thus, under C_{4v} and chiral symmetry, $|C_\pm\rangle$ must both have $\epsilon = 0$. By the same argument, all bulk states that fall into the E representation of C_{4v} must have $\epsilon = 0$ under chiral symmetry.

Now, consider a possible hybridization of the corner states $|C_\pm\rangle$ and the bulk states $|B_\pm\rangle$ that form the E representations of C_{4v} into $|\psi_1\rangle = \alpha(|B_+\rangle + \beta|C_\pm\rangle)$, where $\alpha = 1/\sqrt{1+|\beta|^2}$. Due to C_{4v} , there is another state $|\psi_2\rangle = \alpha(|B_-\rangle + \beta|C_\mp\rangle)$ degenerate to $|\psi_1\rangle$. The crucial observation is that $|\psi_1\rangle$ and $|\psi_2\rangle$ are chiral partners of each other, and as such these hybridized states have zero energy. Thus, the states $|\psi_{1,2}\rangle$ are merely arbitrary choices in the highly degenerate subspace of zero energy and do not represent a physical unbreakable hybridization into resonant eigenstates. The prescription for the detection of BICs that we propose here is then sufficient to isolate the corner BICs from the rest of degenerate states.

In the absence of either chiral or C_{4v} symmetry, the hybridized states are not pinned to zero energy, and are thus free to become eigenstates of the system not susceptible of being separated into their corner and bulk constituents (Fig. 4). The unseparable hybridized states, having support in both the corner and the bulk, will eventually attenuate in the presence of bulk loss, which manifests in the complex energy by a non-zero imaginary component. Some of these states are in principle long-lived as they may have more support in the corners rather than in the bulk, and thus constitute resonances of the system. In Fig. 4 we show the conversion of BICs into resonances as we add perturbations to the original Hamiltonian in Eq. 1 that break the simultaneous C_{4v} and chiral symmetries down to only certain indicated symmetries. The perturbations consist of random hopping terms up to next nearest neighbor unit cells that nevertheless preserve the desired symmetries, as detailed in the SI.

In previous studies, one of the possible mechanisms for creating BICs has been attributed to the *separability* of the Hamiltonian into k_x and k_y dependent parts,

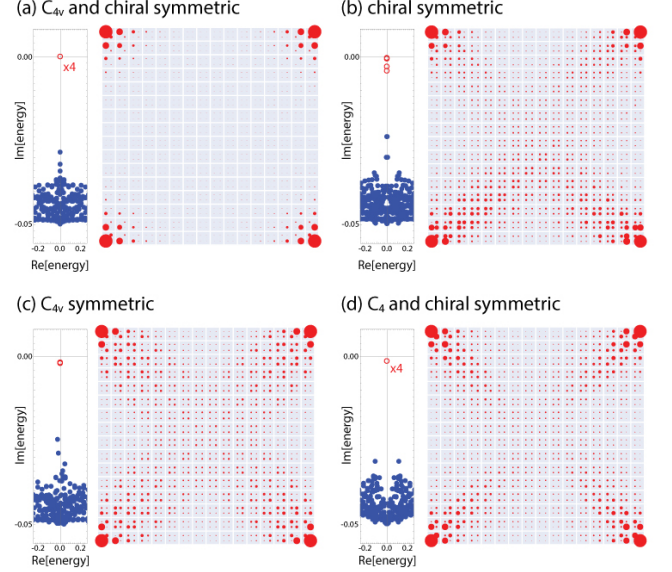


FIG. 4. Breaking the symmetries that protect the BICs. Energy eigenvalues (left panels) and probability densities of the four states whose energies have their imaginary components closest to zero (right panels) under perturbations that preserve certain symmetries: (a) C_{4v} and chiral symmetries, (b) only chiral symmetry, (c) only C_{4v} symmetry, and (d) C_4 and chiral symmetries. In the energy plots, the red hollow circles correspond to the four energies with imaginary components closest to zero (possibly degenerate). Only (a) has BICs; (b), (c), and (d) have corner-localized topological resonances. For all plots, $n = 16$, $n_s = 3$, $\kappa = -5 \times 10^{-2}$ and $t = 0.25$.

i.e., $h(k_x, k_y) = h_x(k_x) + h_y(k_y)$ [68, 69]. Here we show that BICs are protected beyond separability. Specifically, Fig. 4(a) has added perturbations that put the overall Hamiltonian in a non-separable form (see the SI). We also notice that in all cases in Fig. 4 the filling anomaly is preserved, and in (a), (c), and (d), the Wannier centers are still fixed by symmetry to the maximal Wyckoff position $1b$. Thus, we hereby verify that additional symmetries to those required to protect the topological phase and its filling anomaly are required to protect BICs. Resonances, however, will generally exist for the symmetries that protect the topological phase, with a quality factor inversely proportional to the amplitude of the imaginary component of their energies. The recent work of Ref. 66 introduces unrestricted (i.e., symmetry-breaking) noise to their system. Thus, we expect that their numerical method for finding corner-localized states is incapable of properly distinguishing BICs from resonances.

Conclusion — We have shown that corner-localized modes exist in HOTIs even in the absence of a bulk band gap. In the C_2 symmetry protected HOTI phase studied here, we find that BICs exist as long as both C_{4v} and chiral symmetries are preserved. Our work expands the search space (design space) for topological materials (topological metamaterials). Moreover, the unique prop-

erty of coexistence between BICs and bulk states offers a new playground for possible applications of topological phenomena.

Acknowledgements – We thank interesting discussions with Mikael Rechtsman, Jonathan Guglielmon, S. N. Kempkes, and Cristiane Morais Smith. W. A. B. thanks the support of the Eberly Postdoctoral Fellowship at the Pennsylvania State University. A. C. acknowledges the support of National Science Foundation under grant numbers ECCS-1509546 and DMS-1620422 as well as the Charles E. Kaufman foundation under grant number KA2017-91788.

-
- [1] Guido van Miert, Carmine Ortix, and Cristiane Morais Smith, “Topological origin of edge states in two-dimensional inversion-symmetric insulators and semimetals,” *2D Materials* **4**, 015023 (2016).
 - [2] Jun-Won Rhim, Jan Behrends, and Jens H. Bardarson, “Bulk-boundary correspondence from the intercellular zak phase,” *Phys. Rev. B* **95**, 035421 (2017).
 - [3] Guido van Miert and Carmine Ortix, “Excess charges as a probe of one-dimensional topological crystalline insulating phases,” *Phys. Rev. B* **96**, 235130 (2017).
 - [4] W. P. Su, J. R. Schrieffer, and A. J. Heeger, “Solitons in Polyacetylene,” *Phys. Rev. Lett.* **42**, 1698–1701 (1979).
 - [5] Wladimir A. Benalcazar, B. Andrei Bernevig, and Taylor L. Hughes, “Quantized electric multipole insulators,” *Science* **357**, 61–66 (2017).
 - [6] Wladimir A. Benalcazar, B. Andrei Bernevig, and Taylor L. Hughes, “Electric multipole moments, topological multipole moment pumping, and chiral hinge states in crystalline insulators,” *Phys. Rev. B* **96**, 245115 (2017).
 - [7] Zhida Song, Zhong Fang, and Chen Fang, “ $(d - 2)$ -dimensional edge states of rotation symmetry protected topological states,” *Phys. Rev. Lett.* **119**, 246402 (2017).
 - [8] Benjamin J. Wieder and B. Andrei Bernevig, “The axion insulator as a pump of fragile topology,” arXiv:1810.02373 (2018).
 - [9] Guido van Miert and Carmine Ortix, “Higher-order topological insulators protected by inversion and rotoinversion symmetries,” *Phys. Rev. B* **98**, 081110 (2018).
 - [10] Motohiko Ezawa, “Minimal models for wannier-type higher-order topological insulators and phosphorene,” *Phys. Rev. B* **98**, 045125 (2018).
 - [11] Wladimir A. Benalcazar, Tianhe Li, and Taylor L. Hughes, “Quantization of fractional corner charge in C_n -symmetric higher-order topological crystalline insulators,” *Phys. Rev. B* **99**, 245151 (2019).
 - [12] Eunwoo Lee, Rokyeon Kim, Junyeong Ahn, and Bohm-Jung Yang, “Higher-order band topology and corner charges in monolayer graphdiyne,” arXiv preprint arXiv:1904.11452 (2019).
 - [13] Xian-Lei Sheng, Cong Chen, Huiying Liu, Ziyu Chen, YX Zhao, Zhi-Ming Yu, and Shengyuan A Yang, “Two-dimensional second-order topological insulator in graphdiyne,” arXiv preprint arXiv:1904.09985 (2019).
 - [14] Frank Schindler, Marta Brzezińska, Wladimir A Benalcazar, Mikel Iraola, Adrien Bouhon, Stepan S Tsirkin, Maia G Vergniory, and Titus Neupert, “Fractional corner charges in spin-orbit coupled crystals,” arXiv preprint arXiv:1907.10607 (2019).
 - [15] Jiho Noh, Wladimir A. Benalcazar, Sheng Huang, Matthew J. Collins, Kevin P. Chen, Taylor L. Hughes, and Mikael C. Rechtsman, “Topological protection of photonic mid-gap defect modes,” *Nature Photonics* (2018).
 - [16] Marc Serra-Garcia, Valerio Peri, Roman Süssstrunk, Osama R. Bilal, Tom Larsen, Luis Guillermo Villanueva, and Sebastian D. Huber, “Observation of a phononic quadrupole topological insulator,” *Nature* **555**, 342 EP – (2018).
 - [17] Christopher W. Peterson, Wladimir A. Benalcazar, Taylor L. Hughes, and Gaurav Bahl, “A quantized microwave quadrupole insulator with topologically protected corner states,” *Nature* **555**, 346 EP – (2018).
 - [18] Stefan Imhof, Christian Berger, Florian Bayer, Johannes Brehm, Laurens W. Molenkamp, Tobias Kiessling, Frank Schindler, Ching Hua Lee, Martin Greiter, Titus Neupert, and Ronny Thomale, “Topoelectrical-circuit realization of topological corner modes,” *Nature Physics* **14**, 925–929 (2018).
 - [19] Xiang Ni, Matthew Weiner, Andrea Alù, and Alexander B. Khanikaev, “Observation of higher-order topological acoustic states protected by generalized chiral symmetry,” *Nature Materials* **18**, 113–120 (2019).
 - [20] S. N. Kempkes, M. R. Slot, J. J. van den Broeke, P. Capiod, W. A. Benalcazar, D. Vanmaekelbergh, D. Bercioux, I. Swart, and C. Morais Smith, “Robust zero-energy modes in an electronic higher-order topological insulator,” *Nature Materials* (2019), 10.1038/s41563-019-0483-4.
 - [21] Wladimir A. Benalcazar, Jeffrey C. Y. Teo, and Taylor L. Hughes, “Classification of two-dimensional topological crystalline superconductors and majorana bound states at disclinations,” *Phys. Rev. B* **89**, 224503 (2014).
 - [22] Zhongbo Yan, Fei Song, and Zhong Wang, “Majorana corner modes in a high-temperature platform,” *Phys. Rev. Lett.* **121**, 096803 (2018).
 - [23] Qiyue Wang, Cheng-Cheng Liu, Yuan-Ming Lu, and Fan Zhang, “High-temperature majorana corner states,” *Phys. Rev. Lett.* **121**, 186801 (2018).
 - [24] Tao Liu, James Jun He, and Franco Nori, “Majorana corner states in a two-dimensional magnetic topological insulator on a high-temperature superconductor,” *Phys. Rev. B* **98**, 245413 (2018).
 - [25] Yanick Volpez, Daniel Loss, and Jelena Klinovaja, “Second-order topological superconductivity in π -junction rashba layers,” *Phys. Rev. Lett.* **122**, 126402 (2019).
 - [26] Zhiqiang Wu, Zhongbo Yan, and Wen Huang, “Higher-order topological superconductivity: Possible realization in fermi gases and Sr_2RuO_4 ,” *Phys. Rev. B* **99**, 020508 (2019).
 - [27] Thomas Iadecola, Thomas Schuster, and Claudio Chamon, “Non-abelian braiding of light,” *Phys. Rev. Lett.* **117**, 073901 (2016).
 - [28] Jiho Noh, Thomas Schuster, Thomas Iadecola, Sheng Huang, Mohan Wang, Kevin P. Chen, Claudio Chamon, and Mikael C. Rechtsman, *Braiding photonic topological zero modes* (arxiv preprint, arXiv:1907.03208, 2019).
 - [29] Tudor E. Pahomi, Manfred Sigrist, and Alexey A. Soluyanov, *Braiding Majorana corner modes in a two-layer second-order topological insulator* (arxiv preprint,

- arXiv:1904.07822, 2019).
- [30] J. von Neumann and E. Wigner, “Über merkwürdige diskrete eigenwerte,” *Phys. Z.* **30**, 465 (1929).
 - [31] R. L. Schult, D. G. Ravenhall, and H. W. Wyld, “Quantum bound states in a classically unbound system of crossed wires,” *Phys. Rev. B* **39**, 5476–5479 (1989).
 - [32] Nimrod Moiseyev, “Suppression of feshbach resonance widths in two-dimensional waveguides and quantum dots: A lower bound for the number of bound states in the continuum,” *Phys. Rev. Lett.* **102**, 167404 (2009).
 - [33] Lorenz S. Cederbaum, Ronald S. Friedman, Victor M. Ryaboy, and Nimrod Moiseyev, “Conical intersections and bound molecular states embedded in the continuum,” *Phys. Rev. Lett.* **90**, 013001 (2003).
 - [34] F. Ursell, “Trapping modes in the theory of surface waves,” *Math. Proc. Cambridge Philos. Soc.* **47**, 347–358 (1951).
 - [35] D. S. Jones, “The eigenvalues of $\nabla^2 u + \lambda u = 0$ when the boundary conditions are given on semi-infinite domains,” *Math. Proc. Cambridge Philos. Soc.* **49**, 668–684 (1953).
 - [36] M. Callan, C. M. Linton, and D. V. Evans, “Trapped modes in two-dimensional waveguides,” *J. Fluid Mech.* **229**, 51–64 (1991).
 - [37] C. H. Retzler, “Trapped modes: an experimental investigation,” *Appl. Ocean Res.* **4**, 249–250 (2001).
 - [38] P. J. Cobelli, V. Pagneux, A. Maurel, and P. Petitjeans, “Experimental observation of trapped modes in a water wave channel,” *Euro. Phys. Lett.* **88**, 20006 (2009).
 - [39] P. J. Cobelli, V. Pagneux, A. Maurel, and P. Petitjeans, “Experimental study on water-wave trapped modes,” *J. Fluid Mech.* **666**, 445–476 (2011).
 - [40] R. Parker, “Resonance effects in wake shedding from parallel plates: some experimental observations,” *J. Sound Vib.* **4**, 62 (1966).
 - [41] R. Parker, “Resonance effects in wake shedding from parallel plates: calculation of resonant frequencies,” *J. Sound Vib.* **5**, 330 (1967).
 - [42] N. A. Cumpsty and D. S. Whitehead, “The excitation of acoustic resonances by vortex shedding,” *J. Sound Vib.* **18**, 353 (1971).
 - [43] W. Koch, “Resonant acoustic frequencies of flat plate cascades,” *J. Sound Vib.* **88**, 233 (1983).
 - [44] R. Parker and S. A. T. Stoneman, “The Excitation and Consequences of Acoustic Resonances in Enclosed Fluid Flow Around Solid Bodies,” *Proc. Inst. Mech. Eng. C* **203**, 9–19 (1989).
 - [45] D. V. Evans, M. Levitin, and D. Vassiliev, “Existence theorems for trapped modes,” *J. Fluid Mech* **261**, 21–31 (1994).
 - [46] P. Paddon and Jeff F. Young, “Two-dimensional vector-coupled-mode theory for textured planar waveguides,” *Phys. Rev. B* **61**, 2090–2101 (2000).
 - [47] V. Pacradouni, W. J. Mandeville, A. R. Cowan, P. Paddon, Jeff F. Young, and S. R. Johnson, “Photonic band structure of dielectric membranes periodically textured in two dimensions,” *Phys. Rev. B* **62**, 4204–4207 (2000).
 - [48] T. Ochiai and K. Sakoda, “Dispersion relation and optical transmittance of a hexagonal photonic crystal slab,” *Phys. Rev. B* **63**, 125107 (2001).
 - [49] Shanhui Fan and J. D. Joannopoulos, “Analysis of guided resonances in photonic crystal slabs,” *Phys. Rev. B* **65**, 235112 (2002).
 - [50] Chia Wei Hsu, Bo Zhen, Song-Liang Chua, Steven G. Johnson, John D. Joannopoulos, and Marin Soljačić, “Bloch surface eigenstates within the radiation continuum,” *Light Sci. Appl.* **2**, e84 (2013).
 - [51] Chia Wei Hsu, Bo Zhen, Jeongwon Lee, Song-Liang Chua, Steven G. Johnson, John D. Joannopoulos, and Marin Soljačić, “Observation of trapped light within the radiation continuum,” *Nature* **499**, 188–191 (2013).
 - [52] Yi Yang, Chao Peng, Yong Liang, Zhengbin Li, and Susumu Noda, “Analytical Perspective for Bound States in the Continuum in Photonic Crystal Slabs,” *Phys. Rev. Lett.* **113**, 037401 (2014).
 - [53] Bo Zhen, Chia Wei Hsu, Ling Lu, A. Douglas Stone, and Marin Soljačić, “Topological Nature of Optical Bound States in the Continuum,” *Phys. Rev. Lett.* **113**, 257401 (2014).
 - [54] Hengyun Zhou, Bo Zhen, Chia Wei Hsu, Owen D. Miller, Steven G. Johnson, John D. Joannopoulos, and Marin Soljačić, “Perfect single-sided radiation and absorption without mirrors,” *Optica* **3**, 1079–1086 (2016).
 - [55] Xingwei Gao, Chia Wei Hsu, Bo Zhen, Xiao Lin, John D. Joannopoulos, Marin Soljačić, and Hongsheng Chen, “Formation mechanism of guided resonances and bound states in the continuum in photonic crystal slabs,” *Sci. Rep.* **6**, 31908 (2016).
 - [56] Ashok Kodigala, Thomas Lepetit, Qing Gu, Babak Bahari, Yehaiahu Fainman, and Boubacar Kanté, “Lasing action from photonic bound states in continuum,” *Nature* **541**, 196–199 (2017).
 - [57] Wei Zhang, Aaron Charous, Masaya Nagai, Daniel M. Mittleman, and Rajind Mendis, “Extraordinary optical reflection resonances and bound states in the continuum from a periodic array of thin metal plates,” *Opt. Express* **26**, 13195–13204 (2018).
 - [58] Momchil Minkov, Ian A.D. Williamson, Meng Xiao, and Shanhui Fan, “Zero-Index Bound States in the Continuum,” *Phys. Rev. Lett.* **121**, 263901 (2018).
 - [59] Alexander Cerjan, Chia Wei Hsu, and Mikael C. Rechtsman, “Bound States in the Continuum through Environmental Design,” *Phys. Rev. Lett.* **123**, 023902 (2019).
 - [60] Yonatan Plotnik, Or Peleg, Felix Dreisow, Matthias Heinrich, Stefan Nolte, Alexander Szameit, and Mordechai Segev, “Experimental Observation of Optical Bound States in the Continuum,” *Phys. Rev. Lett.* **107**, 183901 (2011).
 - [61] Steffen Weimann, Yi Xu, Robert Keil, Andrey E. Miroshnichenko, Andreas Tünnermann, Stefan Nolte, Andrey A. Sukhorukov, Alexander Szameit, and Yuri S. Kivshar, “Compact Surface Fano States Embedded in the Continuum of Waveguide Arrays,” *Phys. Rev. Lett.* **111**, 240403 (2013).
 - [62] G. Corrielli, G. Della Valle, A. Crespi, R. Osellame, and S. Longhi, “Observation of Surface States with Algebraic Localization,” *Phys. Rev. Lett.* **111**, 220403 (2013).
 - [63] Jordi Gomis-Bresco, David Artigas, and Lluís Torner, “Anisotropy-induced photonic bound states in the continuum,” *Nat. Photon.* **11**, 232 (2017).
 - [64] Samyabrata Mukherjee, Jordi Gomis-Bresco, Pilar Pujol-Closa, David Artigas, and Lluís Torner, “Topological properties of bound states in the continuum in geometries with broken anisotropy symmetry,” *Phys. Rev. A* **98**, 063826 (2018).
 - [65] Bohm-Jung Yang, Mohammad Saeed Bahramy, and Naoto Nagaosa, “Topological protection of bound states against the hybridization,” *Nature Communications* **4**,

- 1524 EP – (2013).
- [66] Ze-Guo Chen, Changqing Xu, Rasha Al Jahdali, Jun Mei, and Ying Wu, “Corner states in a second-order acoustic topological insulator as bound states in the continuum,” *Phys. Rev. B* **100**, 075120 (2019).
 - [67] Although a proper definition of corner-induced filling anomaly requires the vanishing of polarization in insulators, here we do not enforce this requirement as we envision the topology per band instead of the topology below a given Fermi level.
 - [68] M Robnik, “A simple separable hamiltonian having bound states in the continuum,” *Journal of Physics A: Mathematical and General* **19**, 3845–3848 (1986).
 - [69] J. U. Nöckel, “Resonances in quantum-dot transport,” *Phys. Rev. B* **46**, 15348–15356 (1992).
 - [70] Gregory H. Wannier, “Dynamics of band electrons in electric and magnetic fields,” *Rev. Mod. Phys.* **34**, 645–655 (1962).
 - [71] Nicola Marzari and David Vanderbilt, “Maximally localized generalized wannier functions for composite energy bands,” *Phys. Rev. B* **56**, 12847 (1997).
 - [72] Barry Bradlyn, L. Elcoro, Jennifer Cano, M. G. Vergniory, Zhijun Wang, C. Felser, M. I. Aroyo, and B. Andrei Bernevig, “Topological quantum chemistry,” *Nature* **547**, 298 EP – (2017).

Supplementary Information: Bound states in the continuum of higher-order topological insulators

A. Irreducible representations of the energy bands of the lattice model

The Hamiltonian in Eq. 1 has C_{4v} symmetry, which is generated by the simultaneous presence of C_4 symmetry,

$$\hat{r}_4 h(k_x, k_y) \hat{r}_4^\dagger = h(k_y, -k_x), \quad (\text{S1})$$

and reflection symmetry,

$$\hat{M}_x h(k_x, k_y) \hat{M}_x^\dagger = h(-k_x, k_y), \quad (\text{S2})$$

both of which imply also C_2 symmetry as well as reflection symmetries along y -denoted M_y - and along the two diagonals -denoted M_{d1} and M_{d2} . The topology of the crystalline phases of this model can be diagnosed by looking at the representations that the states take at the high-symmetry points (HSPs) of the Brillouin zone. In particular, we are interested in the HSPs Γ and \mathbf{M} , which are invariant under the full group, C_{4v} , as well as the HSPs Γ , \mathbf{X} , and \mathbf{X}' , which are invariant only under the little group C_{2v} . The representations that each of these bands take at these points is given in Table S1.

phase	bands	C_{4v}		C_{2v}		
		Γ	\mathbf{M}	Γ	\mathbf{X}	\mathbf{X}'
$ t < 1$	1	B_2	A_1	a_2	b_1	b_2
	2,3	E	E	$b_1 + b_2$	$a_1 + a_2$	$a_1 + a_2$
	4	A_1	B_2	a_1	b_2	b_1
$ t > 1$	1	B_2	B_2	a_2	a_2	a_2
	2,3	E	E	$b_1 + b_2$	$b_1 + b_2$	$b_1 + b_2$
	4	A_1	A_1	a_1	a_1	a_1

TABLE S1. Symmetry representations at the high symmetry points of the BZ in both topological ($|t| < 1$) and trivial ($|t| > 1$) phases. Irreducible representations (irreps) at Γ and \mathbf{M} are for C_{4v} and irreps at \mathbf{X} and \mathbf{X}' are for C_{2v} . Irreps A_1 , A_2 , B_1 , B_2 , a_1 , a_2 , b_1 , b_2 are one dimensional. Irrep E is two-dimensional.

The irreducible representations in Table S1 have the character tables detailed in Table S2.

irrep	I	C_2	$2C_4$	$2M_v$	$2M_d$
A_1	1	1	1	1	1
A_2	1	1	1	-1	-1
B_1	1	1	-1	1	-1
B_2	1	1	-1	-1	1
E	2	-2	0	0	0

irrep	I	C_2	M_x	M_y
a_1	1	1	1	1
a_2	1	1	-1	-1
b_1	1	-1	1	-1
b_2	1	-1	-1	1

TABLE S2. Character table for the C_{4v} (left) and C_{2v} (right) groups. The irreducible representations at the HSPs of the Brillouin zone for each energy band is shown in Table S1.

Notice that only the group C_{4v} has a two-dimensional irreducible representation, E . This is the representation of the bulk states at zero energy and which coexist with the topological corner BICs.

B. Trivial and topological phases of the model and their Wannier centers

In real space, the topology of the energy bands in the lattice of Fig. 1(a) in the Main Text is described by the positions of their Wannier centers [70, 71]. Although the Block Hamiltonian in Eq. 1 has C_{4v} and chiral symmetries, C_2 symmetry alone suffices to fix the positions of the Wannier centers to one of two disconnected maximal Wyckoff

positions of the lattice: a ‘trivial’ Wannier center for $|t| > 1$, and a ‘topological’ one, for $|t| < 1$. These two phases are in different *atomic limits* [72]. The trivial atomic limit is described by Wannier centers that coincide with the centers of the unit cells [Fig. S1(a)], and the nontrivial atomic limit has Wannier centers at the corners of the unit cells [Fig. S1(b)].

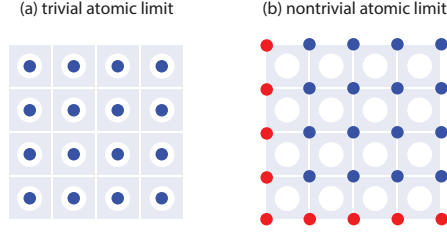


FIG. S1. Wannier center configuration for (a) the trivial phase, $|t| > 1$ and (b) the topological phase, $|t| < 1$. Gray squares are unit cells. Blue and red circles are the Wannier centers. White circles represent the centers of ionic charge. Wannier centers in red are in excess relative to those with closed boundaries.

These two configurations can be diagnosed from the C_2 representations that each of the bands take at the HSPs of the Bloch Hamiltonian, Eq. 1 of the Main Text. Table. S3 compiles these representations, the corresponding Wannier centers, and the nominal corner charge for each band and for both phases.

phase	bands	Γ	X	Y	M	Wannier center	Q^{corner}
$ t < 1$	1	+1	-1	-1	+1	1b	$\frac{e}{4}$
	2,3	-1,-1	+1,+1	+1,+1	-1,-1	1b ($\times 2$)	$\frac{e}{2}$
	4	+1	-1	-1	+1	1b	$\frac{e}{4}$
$ t > 1$	1	+1	+1	+1	+1	1a	0
	2,3	-1,-1	-1,-1	-1,-1	-1,-1	1a ($\times 2$)	0
	4	+1	+1	+1	+1	1a	0

TABLE S3. The C_2 representations of the energy bands at high symmetry points of the BZ in both topological ($|t| < 1$) and trivial ($|t| > 1$) phases.

The topological configuration generates electric dipole moments along both x and y , $\mathbf{P} = (\frac{e}{2}, \frac{e}{2})$. With open boundaries, these moments generate an *edge-induced filling anomaly* [11], an excess in the number of states relative to those with no boundaries. In addition, this configuration has a (nominal) corner-induced filling anomaly [11]: an extra excess or depletion of states caused only in the presence of corners. It is this anomaly that causes the corner localized states at zero energy that, under the right symmetries, constitute topological BICs (if additionally C_{4v} and chiral symmetries are preserved) or topological resonances (if either C_{4v} or chiral are broken) [lower panel for central band in Fig. 1(c) of the Main Text]. We emphasize that not all lattices with $\mathbf{P} = (\frac{e}{2}, \frac{e}{2})$ have a corner-induced filling anomaly. A case in point is the lattice in Fig. 2(e) in Ref. 11.

C. Constraints on the energy spectrum due to chiral symmetry

Consider the energy eigenstate $|u\rangle$ with energy ϵ , such that

$$h|u\rangle = \epsilon|u\rangle. \quad (\text{S3})$$

If the Hamiltonian h has chiral symmetry, $\{h, \Pi\} = 0$, then the state $\Pi|u\rangle$ is an energy eigenstate of h with energy $-\epsilon$,

$$h\Pi|u\rangle = -\Pi h|u\rangle = -\epsilon\Pi|u\rangle \quad (\text{S4})$$

Thus, the energies in a system with chiral symmetry come in pairs $(\epsilon, -\epsilon)$, and their states are related by the chiral operator Π . From this, it follows that states with $\epsilon = 0$ are either eigenstates of Π , in which case have support only in

one sublattice, or come in pairs ($|u\rangle, \Pi|u\rangle$). In the Hamiltonian of Eq. 1, examples of the first case are the individual zero energy corner states, while an example of the second case is the subspace of bulk states at zero energy.

D. Implementing the symmetry-breaking perturbations

To generate the results in Fig. 4 of the Main Text, additional hopping terms were added to the Hamiltonian of Eq. 1. The overall Hamiltonian *before introducing losses in the system*, Eq. (2), is

$$h_T(\mathbf{k}) = h(\mathbf{k}) + \Delta_p h_p(\mathbf{k}), \quad (\text{S5})$$

where Δ_p is the overall strength of the perturbation and

$$\begin{aligned} h_p(\mathbf{k}) = & T_{x1} \cos k_x + T_{x2} \sin k_x + T_{y1} \cos k_y + T_{y2} \sin k_y \\ & + T_1 \cos k_x \sin k_y + T_2 \sin k_x \cos k_y \end{aligned} \quad (\text{S6})$$

is the Hamiltonian of the additional perturbation, which amounts to hopping terms up to next nearest neighbor unit cells. The T matrices are all 4×4 random Hermitian matrices in which each entry has a complex value with a uniform distribution in the range $[0, 1]$. In addition to obeying Hermiticity, the T matrices are subject to certain constraints imposed by the symmetries we are interested in preserving. In what follows we detail examples of the constraints on the T matrices used for the preservation of certain symmetries:

1. For chiral symmetry

Under chiral symmetry, $\Pi h(\mathbf{k}) \Pi = -h(\mathbf{k})$, all T matrices must obey

$$\{T, \Pi\} = 0. \quad (\text{S7})$$

2. For C_4 symmetry

Let us first focus on the nearest neighbor T matrices. To first satisfy C_2 symmetry, $\hat{r}_2 h(k_x, k_y) \hat{r}_2^\dagger = h(-k_x, -k_y)$, we require

$$[T_{x1}, \hat{r}_2] = 0, \quad \{T_{x2}, \hat{r}_2\} = 0. \quad (\text{S8})$$

Now, to satisfy C_4 symmetry, $\hat{r}_4 h(k_x, k_y) \hat{r}_4^\dagger = h(k_y, -k_x)$, we additionally require

$$T_{y1} = \hat{r}_4 T_{x1} \hat{r}_4^\dagger, \quad T_{y2} = -\hat{r}_4 T_{x2} \hat{r}_4^\dagger. \quad (\text{S9})$$

The two next nearest neighbor T matrices are odd under C_2 symmetry. Take first T_1 to obey

$$\{T_1, \hat{r}_2\} = 0, \quad (\text{S10})$$

and then determine T_2 via the constraint due to C_4 symmetry,

$$T_2 = -\hat{r}_4 T_1 \hat{r}_4^\dagger. \quad (\text{S11})$$

3. For reflection symmetry

Under reflection symmetry along x , $\hat{M}_x h(k_x, k_y) \hat{M}_x^\dagger = h(-k_x, k_y)$, four T matrices are even under M_x and two are odd,

$$[T_{x1}, \hat{M}_x] = 0, \quad [T_{y1}, \hat{M}_x] = 0, \quad [T_{y2}, \hat{M}_x] = 0, \quad [T_1, \hat{M}_x] = 0, \quad \{T_{x2}, \hat{M}_x\} = 0, \quad \{T_2, \hat{M}_x\} = 0. \quad (\text{S12})$$

If more than one symmetry is to be preserved, the constraints due to each of them have to be met simultaneously. Once the T matrices are chosen, an inverse Fourier transform allows to implement the hopping terms in real space. For example, the nearest neighbor perturbations along x lead to

$$T_{x1} \cos k_x + T_{x2} \sin k_x \rightarrow \sum_{x,y} \sum_{\alpha,\beta=1}^4 c_{(x,y),\alpha}^\dagger \left(\frac{T_{x1} - iT_{x2}}{2} \right)_{\alpha,\beta} c_{(x+1,y),\beta} + h.c., \quad (\text{S13})$$

where the sum over x and y run over the coordinate of unit cells in the entire lattice.
